Applied Physics Letters ARTICLE scitation.org/journal/apl

Lateral charge carrier transport properties of B-10 enriched hexagonal BN thick epilayers

Cite as: Appl. Phys. Lett. **115**, 072108 (2019); doi: 10.1063/1.5097984
Submitted: 30 March 2019 · Accepted: 19 July 2019 ·
Published Online: 14 August 2019

View Online Export Citation CrossMark

S. Grenadier, A. Maity, J. Li, J. Y. Lin, and H. X. Jiang[a)]

AFFILIATIONS

Department of Electrical and Computer Engineering, Texas Tech University, Lubbock, Texas 79409, USA

[a)]hx.jiang@ttu.edu

ABSTRACT

Neutron detectors based on B-10 enriched hexagonal boron nitride (h-^{10}BN or h-BN) epilayers have demonstrated the highest thermal neutron detection efficiency among solid-state neutron detectors at about 58%. However, many fundamental transport parameters of h-BN, including the room temperature carrier mobility, minority carrier lifetime, and surface recombination velocity, which are essential to the performance of detectors, are still unknown. We report here the carrier drift mobilities (μ) and lifetimes (τ) of both electrons and holes in h-^{10}BN epilayers measured by using a time-of-flight (TOF) technique. Lateral photoconductive type detectors fabricated from a 65 μm thick freestanding h-^{10}BN epilayer were utilized to carry out the TOF measurements, which revealed $\mu_e \sim 34\,cm^2/V\,s$ for electrons and $\mu_h \sim 36\,cm^2/V\,s$ for holes and carrier lifetimes on the order of tens of microseconds. By combining the values of μ measured from TOF with S/μ (the ratio of the surface recombination velocity to mobility) deduced directly from the bias voltage dependence of photocurrent, S for both electrons ($S_e \sim 1.4 \times 10^4$ cm/s) and holes ($S_h \sim 2.7 \times 10^3$ cm/s) in h-^{10}BN has been extracted. The determination of these important fundamental parameters (μ, τ, and S) not only provides a better understanding of the carrier dynamics and electrical transport properties of h-BN but is also valuable for further advancing the development of h-BN materials and devices.

Among the members of the III-nitride material system, hexagonal boron-nitride (h-BN) is substantially less studied and understood. Due to its extraordinary physical properties, such as high bandgap ($E_g > 6$ eV), optical absorption near the band edge, electrical resistivity, and thermal neutron capture cross section, h-BN is very attractive for many emerging technologically significant applications. These include deep UV optoelectronics,[1–15] solid state neutron detectors,[16–20] and single photon emitters.[21–23] This material also has a close lattice match to graphite and is recognized as the most suitable substrate/dielectric separation layer for the construction of van der Waals heterostructures.[24–27] In particular, thermal neutron detectors based on B-10 enriched h-BN (h-^{10}BN) epilayers have demonstrated the highest detection efficiency among solid-state detectors at 58% to date.[19] As such, it is of critical importance to gain a more complete understanding of the electrical transport properties of h-BN, to further advance the development of this material and its applications.

Due to this material's very large energy bandgap and highly resistive nature ($\sim 10^{14}\ \Omega$ cm),[18,19,28] the electrical transport properties of h-BN have been difficult to probe. In particular, it has been challenging to separately measure the charge carrier drift mobility (μ) and lifetime (τ), which are considered two of the most fundamental parameters which characterize the overall material quality of a semiconductor and hence the performance of its associated electronic devices. Hall-effect measurements have been reported but were only possible at high temperatures for h-BN.[28] Moreover, the classical Hall-effect measurement can only provide the mobility of one type of charge carrier (electrons or holes). On the other hand, the combined mobility-lifetime ($\mu\tau$) product can be obtained by measuring and analyzing the photocurrent-applied voltage characteristics using the classical Many's equation under strongly absorbed illumination.[29] The mobility-lifetime product has been extensively utilized as an effective tool for correlating the film properties and device performances for h-BN neutron detector materials[18–20] and for other radiation detectors[30] and solar cell materials.[31] However, the ability to measure separately the carrier mobility and lifetime for both electrons and holes would not only enable the decoupling of these two important parameters but also provide deeper insights into the electrical transport properties and carrier dynamics of these materials. Moreover, for the purposes of further improving the material quality and device performance, it is important to know the carrier mobility and lifetime in the same sample/device separately so that better decisions can be made in terms of optimization of material growth and device processing parameters.

Furthermore, knowing the values for μ and τ separately for both types of carriers (electrons and holes) would also allow the determination of the surface recombination velocities (S) of both types of carriers, which are important fundamental parameters and strongly influence the overall performance of semiconductor devices.

Time-of-flight (TOF) is one of the most commonly used techniques for the exploration of the electrical transport properties of organic and inorganic semiconductor materials.[32–35] In TOF measurements, a pulsed laser generates charge carriers at one end of the sample which are drifted across the material with the aid of an applied electric field. Through the monitoring of photocurrent from the sample with a current sensing resistor and an oscilloscope, two peaks are observable, one for the charge carriers that are immediately collected at the electrode on the charge generating layer and another for the opposite electrode where the charge carriers drifting through the material are collected. The second peak arrives at a delayed time known as the transit time (T_t). With the known electric field strength E, transit time T_t, and drift distance D, the drift mobility of the charge carrier can be determined by the following equation:[34]

$$\mu = \frac{D}{E \cdot T_t}. \quad (1)$$

The mobilities of electrons and holes can be measured separately by changing the direction of the applied electric field. In this work, we report the characterization of charge carrier mobilities and lifetimes of both types of carriers (electrons and holes) in h-^{10}BN epilayers by TOF, which are highly relevant to the further development of h-BN and its associated devices and applications.

A 65 μm thick h-^{10}BN epilayer was grown by metal organic chemical vapor deposition (MOCVD) on a 4-in. diameter c-plane sapphire (Al_2O_3) substrate. The detailed growth procedures have been discussed in previous publications.[18,19] Due to the large difference in thermal expansion coefficients between h-BN and the sapphire substrate, h-BN epilayers tend to mechanically separate from the sapphire substrate after growth, during cooling down, if the thickness of h-BN is large enough. This phenomenon results in the creation of a free-standing wafer of h-BN. A photoconductive type detector in a lateral geometry was fabricated by affixing a diced piece of the h-^{10}BN sample to sapphire and depositing Ni (100 nm)/Au (40 nm) bilayer contacts on two edges of the sample by e-beam evaporation.[19] Wire bonding was then performed to create an electrical connection between the deposited metal contacts and the pads of a semiconductor device package. A microscopy image of a fabricated device (with an exposed area of 2 mm × 4 mm) is shown in Fig. 1(a). The dark areas on both sides of the structure are the Ni/Au bilayer metal contacts. Figure 1(b) shows the measured I-V characteristics of the leakage (or dark) current of the detector, exhibiting an extremely low leakage current which is near the measurement limit of the electrometer up to a bias voltage of 500 V due to the highly resistive nature of this material. Figure 1(c) shows a typical Raman spectrum of h-^{10}BN epilayers.[36] The observed mode at 1370 cm^{-1} is attributed to the E_{2g} symmetry vibration in h-BN, corresponding to the in-plane stretch of B and N atoms,[37] which can be inferred as an indication of a good layered structure formation. The typical linewidth of the x-ray diffraction (XRD) rocking curves of the (0002) diffraction peak for MOCVD grown h-BN epilayers is about 380 arc sec.[12]

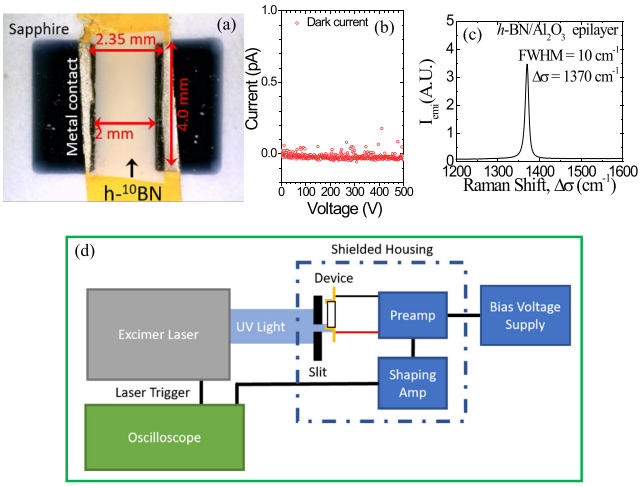

FIG. 1. (a) Optical microscopy image of a lateral photoconductive h-^{10}BN detector structure with Ni/Au metal bilayer contacts deposited on two edges. The width of the material is 2.35 mm, and the gap between two electrodes on the top surface of the structure is 2 mm. (b) Measured dark current up to an applied bias voltage of 500 V. (c) Raman spectrum of a h-^{10}BN epilayer.[36] (d) Schematic of the time-of-flight (TOF) measurement setup employed in this study.

The TOF measurement setup is schematically shown in Fig. 1(d). We used a charge sensitive preamplifier in conjunction with a shaping amplifier instead of a simple current sensing resistor in the TOF setup to enhance the photogenerated charge carrier signals from the highly resistive h-^{10}BN epilayer. Because of the linear relationship between the voltage output and the instantaneous charge collection in the material under test, the charge carrier trapping time (τ) can also be directly measured from the voltage height of the second peak. These results are further verified by comparing the product of the separately measured μ and τ from TOF with the combined $\mu\tau$ product measured directly by fitting the bias voltage dependent photocurrent with Many's equation.[29] To perform the TOF measurement, the detector was placed in a shielded housing with the charge sensitive preamplifier and shaping amplifier. An excimer laser (193 nm) was used to generate the excitation light pulses at a repetition rate of 1 Hz. Due to the large optical absorption coefficient of 7.5×10^5 cm^{-1} for the above bandgap photons,[5,9] nearly all the above incoming bandgap light was absorbed within the first ~70 nm of h-BN material. A 300 μm × 4 mm metal slit was used to allow light to enter and illuminate only near one of the metal contacts of the structure. The photogenerated charge carriers were then drifted by the applied electric field. The shaping time of the amplifier was chosen to be orders of magnitude shorter than the measured transit time. A Keithley sourcemeter was used to supply the bias voltage, and an Agilent oscilloscope with a time resolution of 15 ns was used to record the output waveforms from the shaping amplifier. The excimer laser's output trigger signal was used to provide a trigger to the oscilloscope for recording the waveform data.

Waveforms were measured and exported from the oscilloscope under different bias voltages (V) between 50 and 150 V, corresponding to electric field strengths (E) between 250 and 750 V/cm with a distance of 2 mm between the inside edges of the two electrodes. The direction of the applied electric field was reversed to allow separate

data collection as shown in the top panels of Fig. 2(a) for electrons and Fig. 2(b) for holes. In Figs. 2(a) and 2(b), the carrier transit times are indicated by arrows pointing to the second peak which corresponds to the arrival time of the charge carrier that is drifted across the sample. The bottom panels of Figs. 2(a) and 2(b) show the plots of measured transit time vs E for electrons and holes, respectively. The transit time was obtained by performing a Lorentzian fit around the second peak and extracting the location of the peak's center. Examples of this fitting at an applied bias voltage of 90 V are shown in the insets of the bottom panels of Figs. 2(a) and 2(b). It is clear that the transit time for the drifted charge carriers decreases with increasing V or E. By dividing the transit distance (D = 2 mm) by the transit time of the drifted carriers, we were able to obtain the carrier velocity vs E for electrons and holes, as shown in Fig. 3(a). The slope of the linear fit of these data provides us with the mobility of the drifted carriers. From this, we

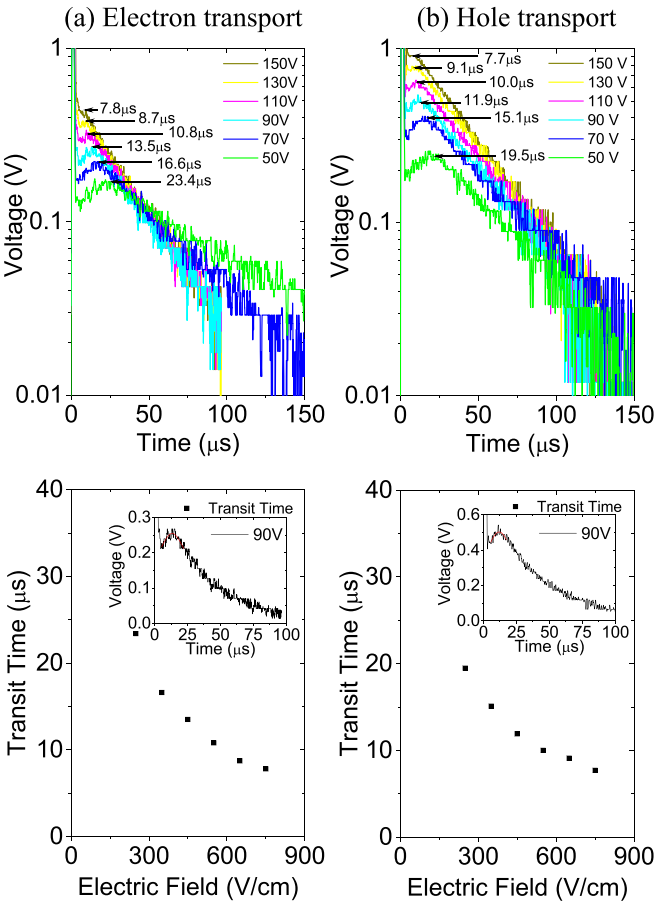

FIG. 2. (a) Top panel: recorded temporal responses of output voltage for electron transport under different bias voltages (V) between 50 and 150 V. Bottom panel: transit time as a function of the applied electric field for photogenerated electrons. (b) Top panel: recorded temporal responses of output voltage for hole transport under different V between 50 and 150 V. Bottom panel: transit time as a function of the applied electric field for photogenerated holes. The insets of both (a) and (b) show measured transient responses at 90 V with the Lorentzian peak fitting performed on the second peak.

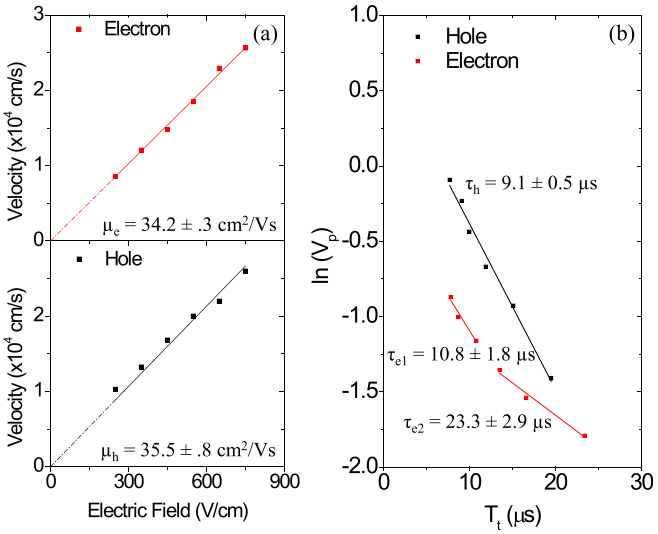

FIG. 3. (a) Carrier drift velocity vs applied electric field for (top panel) electrons and (bottom panel) holes. The slope of the linear fit of the data provides the carrier drift mobility of h-^{10}BN in the lateral direction. (b) ln (V_p) (peak voltage) vs T_t (transit time) for electrons and holes. The linear fit of the data provides the trapping lifetime of drifted photogenerated carriers in h-BN.

obtained drift mobilities of $\mu_e = 34.2\,cm^2/V\,s$ for electrons and $\mu_h = 35.5\,cm^2/V\,s$ for holes.

As mentioned previously, the peak voltage is a measure of instantaneous peak charge collection. Using this information, we were able to determine the charge carrier lifetime (τ). This was done by examining the correlation between the peak voltage (V_p) and transit time shown in Fig. 3(b). It was observed that V_p increases as the transit time decreases (V_B increases). The inverse of the slope of the linear fit of ln (V_p) vs T_t is the lifetime of the drifted carrier in the sample. The measured carrier lifetime for holes was $\tau_h = 9.1\ \mu s$, whereas the data points collected for electron transport exhibited two slopes, indicating the possible presence of electrons at two different energy levels for photoexcitation, one with a lifetime of $\tau_{e1} = 10.8\ \mu s$ and the other with a lifetime of $\tau_{e2} = 23.3\ \mu s$. We would like to point out that the peak voltage positions obtained from the Lorentzian peak fitting are consistent with those obtained by directly reading the apparent peak positions in the row data for both electron transport and hole transport. Moreover, the same methodology applied in the same applied voltage range revealed only a single decay lifetime for holes. We therefore are confident of our measured data shown in Fig. 3. However, the mechanism of two different electron lifetimes still requires further studies.

The surface recombination velocity (S) is another important parameter that strongly impacts the device performance but remains unknown so far for h-BN. With the measured values of μ from the TOF technique, it is possible to extract the values of S for both electrons and holes from the photocurrent-voltage characteristics of the same sample. We have recorded and analyzed the photocurrent as a function of the applied bias voltage for both electron conduction and hole conduction. Figure 4 plots the photocurrent-voltage characteristics for electrons and holes and their fits with Many's equation for

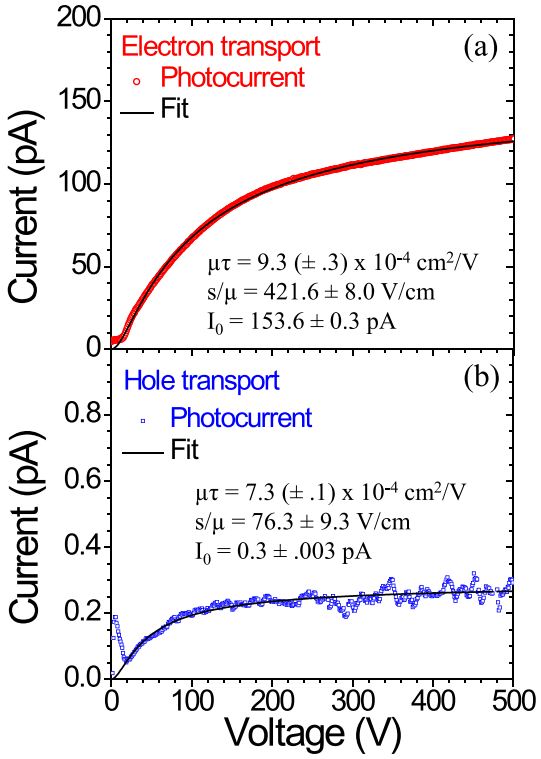

FIG. 4. Photocurrent-voltage characteristics for (a) electrons and (b) holes. The fitted values of the $\mu\tau$ product, S/μ, and saturation current (I_0) are indicated inside the figures.

insulating semiconductors under strongly absorbed illumination as described below,[29]

$$I(V) = I_0\eta_c(V) = I_0\left[\frac{\mu\tau V\left(1 - e^{-\frac{D^2}{\mu\tau V}}\right)}{D^2\left(1 + \frac{SD}{\mu V}\right)}\right], \quad (2)$$

where η_c(V) defines the charge collection efficiency at a bias voltage (V) applied between the two electrodes, D is the carrier transit distance, I_0 is the saturation current, S is the surface recombination velocity, and μ is the carrier drift mobility. It should be noted that Eq. (2) takes into consideration both the effects of the surface recombination (the denominator term) and charge trapping by bulk defects (the numerator term).[29] The fitted value of S/μ using this technique was about 420 V/cm for electrons. This provides an S_e of about 1.4×10^4 cm/s for electrons. For holes, the fitted value of S/μ was about 76 V/cm, which yields a value of S_h of about 2.7×10^3 cm/s. The charge collection efficiency (η_c) at 500 V limited by the numerator term of Eq. (2) (due to the effect of charge trapping by bulk defects) is greater than 99%, whereas η_c limited by the denominator term of Eq. (2) (due to the effect of surface recombination) is about 85%.

The $\mu\tau$ product values obtained from fitting the photocurrent-voltage characteristics with Eq. (2) are also in a reasonable agreement with those acquired using TOF. For electron transport, the longer lifetime component $\mu_e\tau_{e2} = 8.0 \times 10^{-4}$ cm^2/V obtained from TOF is quite consistent with a value of $\mu_e\tau_e = 9.3 \times 10^{-4}$ cm^2/V extracted from the photocurrent-voltage characteristics shown in Fig. 4(a). For hole transport, $\mu_h\tau_h$ is $\sim 3.2 \times 10^{-4}$ cm^2/V measured by TOF and $\sim 7.3 \times 10^{-4}$ cm^2/V deduced from the photocurrent-voltage characteristics shown in Fig. 4(b). An interesting question is concerned with the observation of the exciton dissociation effect, even though the exciton binding energy in *h*-BN is rather large.[2,3,38] This behavior seems to resemble the high efficiency of free charge carrier generation in organic materials, in which excitons can dissociate via various mechanisms despite their huge binding energies (can be as large as >1 eV).[39] In h-BN, the presence of local fields induced by ionized defects (donors and acceptors) could enhance the long-range exciton dissociation[38] as in the case of organic solar cells. Moreover, the increased exciton recombination lifetime under an applied electric field could also enhance the dissociation of excitons. However, this phenomenon of high free charge carrier generation efficiency under a moderate applied electric field in h-BN remains to be understood.

In summary, the drift mobilities and lifetimes in h-^{10}BN epilayers were measured for both electrons and holes by TOF. Combining the results from TOF with those from the photocurrent-voltage characteristics, we were also able to extract the values of the surface recombination velocities of electrons and holes in h-BN. We observed the possible presence of two different electron lifetimes in our material which may indicate the existence of multiple electron excitation states in h-BN. Finding ways to further enhance the carrier mobilities and reduce the surface recombination velocities in h-BN is critical to the improvement of h-BN devices including deep UV emitters, deep UV detectors and neutron detectors.

This research was supported by DOE ARPA-E (No. DE-AR0000964). The DOE NNSA SSAA program (No. DE-NA0002927) supported the initial h-BN detector development efforts. H. X. Jiang and J. Y. Lin are grateful to the AT&T Foundation for the support of Ed Whitacre and Linda Whitacre endowed chairs.

REFERENCES

[1]K. Watanabe, T. Taniguchi, and H. Kanda, Nat. Mater. **3**, 404 (2004).
[2]B. Arnaud, S. Lebègue, P. Rabiller, and M. Alouani, Phys. Rev. Lett. **96**, 026402 (2006).
[3]L. Wirtz, A. Marini, and A. Rubio, Phys. Rev. Lett. **96**, 126104 (2006).
[4]Y. Kubota, K. Watanabe, O. Tsuda, and T. Taniguchi, Science **317**, 932 (2007).
[5]T. Sugino, K. Tanioka, S. Kawasaki, and J. Shirafuji, Jpn. J. Appl. Phys., Part 2 **36**, L463 (1997).
[6]K. Watanabe and T. Taniguchi, Phys. Rev. B **79**, 193104 (2009).
[7]R. Dahal, J. Li, S. Majety, B. N. Pantha, X. K. Cao, J. Y. Lin, and H. X. Jiang, Appl. Phys. Lett. **98**, 211110 (2011).
[8]S. Majety, J. Li, X. K. Cao, R. Dahal, B. N. Pantha, J. Y. Lin, and H. X. Jiang, Appl. Phys. Lett. **100**, 061121 (2012).
[9]J. Li, S. Majety, R. Dahal, W. P. Zhao, J. Y. Lin, and H. X. Jiang, Appl. Phys. Lett. **101**, 171112 (2012).
[10]D. A. Laleyan, S. Zhao, S. Y. Woo, H. N. Tran, H. B. Le, T. Szkopek, H. Guo, G. A. Botton, and Z. Mi, Nano Lett. **17**, 3738 (2017).
[11]X. Yang, S. Nitta, K. Nagamatsu, S. Y. Bae, H. J. Lee, Y. Liu, M. Pristovsek, Y. Honda, and H. Amano, J. Cryst. Growth **482**, 1 (2018).
[12]H. X. Jiang and J. Y. Lin, ECS J. Solid State Sci. Technol. **6**, Q3012 (2017).
[13]H. Liu, J. Meng, X. Zhang, Y. Chen, Z. Yin, D. Wang, Y. Wang, J. You, M. Gao, and P. Jin, Nanoscale **10**, 5559 (2018).
[14]X. Li, M. B. Jordan, T. Ayari, S. Sundaram, Y. E. Gmili, S. Alam, M. Alam, G. Patriarche, P. L. Voss, J. P. Salvestrini, and A. Ougazzade, Sci. Rep. **7**, 786 (2017).

[15]M. Sajjad, W. M. Jadwisienczak, and P. Feng, Nanoscale **6**, 4577 (2014).
[16]J. Uher, S. Pospisil, V. Linhart, and M. Schiebar, Appl. Phys. Lett. **90**, 124101 (2007).
[17]F. P. Doty, U.S. patent 6,727,504 (27 April 2004).
[18]A. Maity, T. C. Doan, J. Li, J. Y. Lin, and H. X. Jiang, Appl. Phys. Lett. **109**, 072101 (2016).
[19]A. Maity, S. J. Grenadier, J. Li, J. Y. Lin, and H. X. Jiang, J. Appl. Phys. **123**, 044501 (2018); Appl. Phys. Lett. **114**, 222102 (2019).
[20]K. Ahmed, R. Dahal, A. Weltz, J. J.-Q. Lu, Y. Danon, and I. B. Bhat, Appl. Phys. Lett. **110**, 023503 (2017).
[21]R. Bourrellier, S. Meuret, A. Tararan, O. Stephan, M. Kociak, L. H. G. Tizei, and A. Zobelli, Nano Lett. **16**, 4317 (2016).
[22]T. Q. P. Vuong, G. Cassabois, P. Valvin, A. Ouerghi, Y. Chassagneux, C. Voisin, and B. Gil, Phys. Rev. Lett. **117**, 097402 (2016).
[23]T. Tran, K. Bray, M. J. Ford, M. Toth, and I. Aharonovich, Nat. Nanotechnol. **11**, 37 (2016).
[24]A. K. Geim and I. V. Grigorieva, "Van der Waals heterostructures," Nature **499**, 419 (2013).
[25]C. R. Dean, A. F. Young, I. Meric, C. Lee, L. Wang, S. Sorgenfrei, K. Watanabe, T. Taniguchi, P. Kim, K. L. Shepard, and J. Hone, Nat. Nanotechnol. **5**, 722 (2010).
[26]L. Britnell, R. V. Gorbachev, R. Jalil, B. D. Belle, F. Schedin, A. Mishchenko, T. Georgiou1, M. I. Katsnelson, L. Eaves, S. V. Morozov, N. M. R. Peres, J. Leist, A. K. Geim, K. S. Novoselov, and L. A. Ponomarenko, Science **335**, 947 (2012).
[27]C. Dean, A. F. Young, L. Wang, I. Meric, G.-H. Lee, K. Watanabe, T. Taniguchi, K. Shepard, P. Kim, and J. Hone, Solid State Commun. **152**, 1275 (2012).
[28]T. C. Doan, J. Li, J. Y. Lin, and H. X. Jiang, AIP Adv. **4**, 107126 (2014).
[29]A. Many, J. Phys. Chem. Solids **26**, 575 (1965).
[30]T. Takahashi and S. Watanabe, IEEE Trans. Nucl. Sci. **48**, 950 (2001).
[31]N. Beck, N. Wyrsch, C. Hof, and A. Shah, J. Appl. Phys. **79**, 9361 (1996).
[32]Z. P. Guan, J. Z. Li, G. Y. Zhang, S. X. Jin, and X. M. Ding, Semicond. Sci. Technol. **15**, 51 (2000).
[33]J. Isberg, J. Hammersberg, E. Johansson, T. Wikström, D. J. Twitchen, A. J. Whitehead, S. E. Coe, and G. A. Scarsbrook, Science **297**, 1670 (2002).
[34]B. Chen, C. S. Lee, S. T. Lee, P. Webb, Y. C. Chan, W. Gambling, H. Tian, and W. Zhu, Jpn. J. Appl. Phys., Part 1 **39**(3R), 1190 (2000).
[35]E. Lebedev, T. Dittrich, V. Petrova-Koch, S. Karg, and W. Brütting, Appl. Phys. Lett. **71**, 2686 (1997).
[36]X. Z. Du, M. R. Uddin, J. Li, J. Y. Lin, and H. X. Jiang, Appl. Phys. Lett. **110**, 092102 (2017).
[37]R. J. Nemanich, S. A. Solin, and R. M. Martin, Phys. Rev. B **23**, 6348 (1981).
[38]T. C. Doan, J. Li, J. Y. Lin, and H. X. Jiang, Appl. Phys. Lett. **109**, 122101 (2016).
[39]D. Caruso and A. Troisi, Proc. Natl. Acad. Sci. U. S. A. **109**, 13498 (2012).